Influence of lattice distortions in classical spin systems

D. C. Cabra,[1,2,3] M. Moliner,[1] and F. Stauffer[1]
[1]*Laboratoire de Physique Théorique, Université Louis Pasteur, 3 rue de l'Université, F-67084 Strasbourg Cedex, France*
[2]*Departamento de Física, Universidad Nacional de la Plata, Casilla de Correo 67, (1900) La Plata, Argentina*
[3]*Facultad de Ingeniería, Universidad Nacional de Lomas de Zamora, Cno. de Cintura y Juan XXIII, (1832) Lomas de Zamora, Argentina*

(Received 20 March 2006; revised manuscript received 22 June 2006; published 25 July 2006)

We investigate a simple model of a frustrated classical spin chain coupled to adiabatic phonons under an external magnetic field. A thorough study of the magnetization properties is carried out both numerically and analytically. We show that already a moderate coupling with the lattice can stabilize a plateau at 1/3 of the saturation and discuss the deformation of the underlying lattice in this phase. We also study the transition to saturation where either a first- or second-order transition can occur, depending on the coupling's strength.

DOI: 10.1103/PhysRevB.74.014428 PACS number(s): 75.10.Jm, 75.10.Pq, 75.60.Ej

I. INTRODUCTION AND MOTIVATION

The study of frustrated spin systems continues to be a subject of intense research, in particular in low dimensions where the effect of quantum fluctuations is more dramatic, leading to fairly rich phase diagrams. On the one hand, one-dimensional frustrated quantum spin systems are in general well under control, mainly thanks to the availability of powerful techniques like bosonization[1] and density matrix renormalization group (DMRG).[2–4] On the other hand, these techniques have unfortunately not been successfully generalized to the two-dimensional case and there is then a strong need for the development of useful techniques to analyze these systems.[5]

A standard way to study quantum spin systems is to start from the analysis of the classical (large S) limit and then try to include the effects of quantum fluctuations in a systematic manner.[6] In certain cases, this procedure can lead to a reasonable description of an otherwise intractable problem. Related to this, the interplay between frustration and classical phonons has been shown to lead to interesting features, even for the classical spin system on the pyrochlore lattice,[8] like the stabilization of a magnetization plateau at 1/2 of saturation. Then, a natural question that arises is whether the classical limit could be generally a good starting point to tackle the issue of the interplay between frustration and lattice deformations and its incidence on the appearance of magnetization plateaus. In the present paper we analyze this point by focusing on a one-dimensional J_1-J_2 model coupled to classical phonons, where both the quantum and classical situations can be analyzed and compared. This and related problems have been studied in the past,[9–11] but to the best of our knowledge, the magnetization properties have not been analyzed so far.

The quantum version of this model has been studied in a recent article,[12] where it has been shown that the effects of lattice distortions coupled to a given frustrated quantum spin system can lead to new phases, in particular to plateaus and jumps in the magnetization curve. Although plateau phases are also present in the pure spin system,[13] it has been shown that lattice effects can lead to the enhancement of these phases under certain circumstances. It is worthwhile mentioning that inorganic compounds like $CuGeO_3$ (Ref. 14) and LiV_2O_5 (Refs. 15 and 16) are well described by the J_1-J_2 model, rendering its study both theoretically and experimentally relevant. Values for the exchange integrals, such as $J_1 \approx 160$ K and the ratio $J_2/J_1 \approx 0.36$, have also been proposed for copper germanate.[17]

We shall address the question of whether the effects of these lattice deformations can already lead to interesting magnetization properties at the classical level. The main motivation for the present study is to analyze the origin of such plateaus in the particular case of a classical zigzag chain. Although this case is particularly simple and the quantum model can be treated using bosonization, understanding the role of lattice deformations for classical spins could lead to a way to study more involved situations, such as two-dimensional frustrated systems, where analytical techniques are not as powerful as in one-dimensional frustrated systems as indicated earlier.

Let us consider the J_1-J_2 frustrated chain coupled to adiabatic phonons

$$\mathcal{H} = \frac{1}{2}K\sum_i \delta_i^2 + J_1\sum_i (1-\tilde{A}_1\delta_i)\boldsymbol{S}_i\cdot\boldsymbol{S}_{i+1} + J_2\sum_i \boldsymbol{S}_i\cdot\boldsymbol{S}_{i+2} - H\sum_i S_i^z. \quad (1)$$

In the previous Hamiltonian, we chose to modulate only the nearest-neighbor (NN) interaction term, and to consider there is no effect on the next-to-nearest-neighbor (NNN) coupling. This minimizes the number of parameters in the Hamiltonian. We have, however, checked that the inclusion of such a modulation on the NNN couplings does not belie our main conclusions.

In the classical system, phonons can be integrated out,[18] leading to an extra quartic interaction among the spins. The effective Hamiltonian, written in units of J_1, reads

$$\mathcal{H}_{\text{eff}} = \sum_i \left[\boldsymbol{S}_i\cdot\boldsymbol{S}_{i+1} + \alpha\boldsymbol{S}_i\cdot\boldsymbol{S}_{i+2} - \frac{A_1^2}{2}(\boldsymbol{S}_i\cdot\boldsymbol{S}_{i+1})^2\right] - h\sum_i S_i^z, \quad (2)$$

where the following reduced quantities, $\alpha = J_2/J_1$, $A_1 = \frac{\tilde{A}_1}{(K/J_1)^{1/2}}$, and $h = H/J_1$ were defined. Even though one should

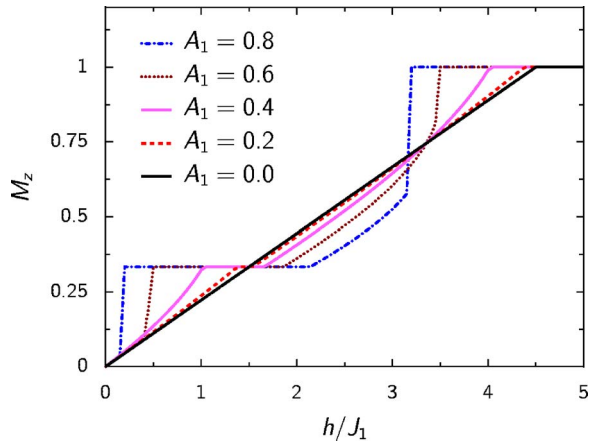

FIG. 1. (Color online) Magnetization curves $M(h)$ for $N=30$ spins with $\alpha=0.5$ and $A_1=0.0,\ldots,0.8$ in steps of 0.2. Periodic boundary conditions are applied on the chain. The system is gradually cooled to $T\approx 0$ over 3×10^6 Monte Carlo sweeps.

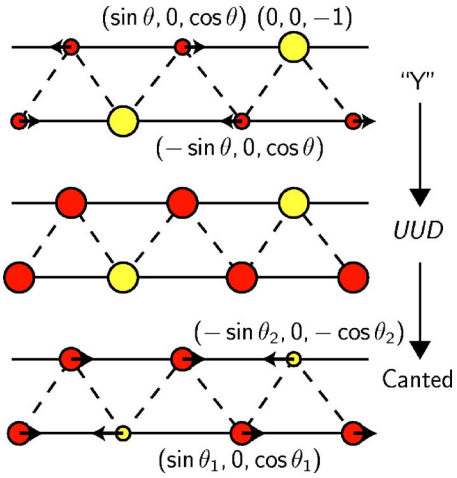

FIG. 2. (Color online) Configurations observed in the low-field, the 1/3 magnetization plateau, and the high-field regions. The chain is viewed in the xy plane. The arrows denote the projection of $\boldsymbol{S}_i$ in this plane, whereas the circles represent the S_z component: red (gray) for $S_z>0$, yellow (light gray) otherwise, and radius proportional to $|S_z|$. The parametrization of the states is given for each configuration.

study the effect of the elastic constants K and $\tilde{A}_1$ separately, we will focus on the reduced coupling A_1 whenever possible, reducing the number of parameters to a manageable size.

In Sec. II we study the magnetic phase diagram using numerical and analytical techniques. We pinpoint a region in the parameters space where a plateau appears at $M_z=1/3$ only. This should be contrasted with the quantum model, which shows in addition a clear $M_z=0$ plateau in a wide region of the parameters space, and another at $M_z=1/2$ in a narrower region. Looking into the detailed structure of the ground state at these plateaus, one can understand this discrepancy in the following way: the structure at $M_z=1/3$ is of the "up-up-down" (UUD) type, indicating a classical plateau,[20] while in the $M_z=0$ case the singlet structure can be identified with a quantum one.

In Sec. III we discuss the transition to saturation, which is found to be either of first or second order depending on the ratio between frustration α and effective lattice coupling A_1.

II. 1/3 MAGNETIZATION PLATEAU

Let us analyze the magnetic phase diagram of the model (2). In the absence of an external magnetic field and when $A_1<\sqrt{4\alpha-1}$, the ground state is a spiral with a pitch angle θ given by $\cos\theta=1/(A_1^2-4\alpha)$. Its energy is

$$E_{\text{spiral}}=\frac{1}{2}\cos\theta-\alpha. \tag{3}$$

When $A_1>\sqrt{4\alpha-1}$ the ground state is Néel ordered. The magnetization curves of this system show interesting features, which vary depending on the relation between α and A_1, as we discuss below.

In Fig. 1 we represent $M(h)$ for a fixed value of the frustration $\alpha=1/2$ and different values of the spin-phonon coupling A_1. The data were obtained using classical Monte Carlo (MC) based on the usual Metropolis algorithm. Starting at high temperatures we perform several thousands of MC sweeps, and then cool down the system to a fraction of the initial temperature. This procedure is then repeated, slowly annealing the system to zero temperature. We observe that a steady magnetization plateau at 1/3 appears as soon as the coupling to the lattice is slightly turned on, whose length increases with A_1. One can notice that the way the system enters the plateau from the low-field side and eventually saturates differs depending on the effective lattice coupling A_1. For $A_1\gtrsim 0.6$ the two are first-order transitions. Another interesting characteristic seen in Fig. 1 is that all curves represented (except one) cross at the same field $h\approx 3.35$ for which $M_\times=M(h)\approx 0.745$. We shall discuss this point at the end of Sec. III. This brief overview suggests that the coupling with the phonons stabilizes the state at $M_z=1/3$. Since the plateaus are observed at zero temperature, we can fairly assume that this effect is energy driven.

After this numerical preamble, it is time to derive some analytical predictions on the characteristics of the magnetization plateau. For this purpose, we need to find out which states describe the system in the low- and high-field regions around $M_z=1/3$. It is not surprising that in the plateau phase the system adopts the UUD state, but it will be a crucial point in our discussion as we shall see later. In this state, the spins are aligned along the z axis, two up spins alternating with one down spin which is precisely the structure seen at the 1/3 plateau in the quantum model.[12]

The classical MC data indicate that the situation in the low-field region is more complicated. On the one hand, the transition to the UUD state can occur at a very low field, where the system is not far from its zero-field ground state. Then, there is no small unit cell structure providing a good description of the system, as the spiral structure still prevails. On the other hand, when the transition is smooth in the low-field region, a plausible assumption is to consider that the system adopts a coplanar "Y" configuration parametrized by a single angular degree of freedom θ (see Fig. 2). The unit

cell energy for this state reads

$$E_Y(\theta) = (1+\alpha)[2\cos\theta(\cos\theta - 1) - 1] - \frac{A_1^2}{2}[2\cos^2\theta + (2\cos^2\theta - 1)^2] - h(2\cos\theta - 1). \quad (4)$$

This expression can be minimized for any set of the parameters h, α, and A_1. As the magnetic field increases, the solution will eventually yield $\theta=0$ corresponding to the UUD state. This configuration is always a solution of $\partial_\theta E_Y(\theta)=0$, but it is only a minimum of the energy when $h \geq h_Y = 1+\alpha - 3A_1^2$. We should emphasize that this discussion only makes sense whenever h_Y is positive. For a given value of the magnetic field, there can be other solutions satisfying

$$h = (1+\alpha)(2\sqrt{1-X^2} - 1) - A_1^2(3-4X^2)\sqrt{1-X^2}, \quad (5)$$

where $X=\sin\theta$ (assuming $\cos\theta > 0$). The study of Eq. (5) boils down to finding the sign of a polynomial expression. Introducing $\Delta = 2(1+\alpha) - 11A_1^2$, we can show that when $\Delta \geq 0$ there is exactly one more extremum of the energy for $h \leq h_Y$ and that it is always a minimum. This solution becomes precisely the UUD state at $h=h_Y$. Under these assumptions, we can conclude that the critical field for which we recover $M_z=1/3$ from the low field regime is

$$h_{c1} = 1 + \alpha - 3A_1^2, \quad \Delta \geq 0. \quad (6)$$

This can be compared to our MC results. For instance, the data for $\alpha=0.5$ and $A_1=0.4$, which correspond to the solid pink (gray) curve in Fig. 1, allow us to obtain a precise estimate for h_{c1} at $T \approx 0$. We get $h_{c1}=1.02\pm0.01$. For this set of parameters, Δ is positive so that we are ruled by the previous assumptions. The analytical expression (6) yields $h_{c1}=1.02$, which is in excellent agreement with the simulations.

For $\Delta < 0$ there can be up to two extra solutions when $h \geq h_Y$. As there is always one solution that never turns out to become UUD for a certain value of the magnetic field, we ought to perform a detailed comparison of the two solutions' energies in order to conclude. We shall not step further into this discussion, which can nevertheless be conducted numerically using the previous analytical expressions. For instance, we performed it when $\alpha=1/2$, $A_1=0.6$, leading to $h_{c1} \approx 0.46$. This is in good agreement with the MC data which gives $h_{c1} \approx 0.47 \pm 0.01$ (the dotted curve in Fig. 1). It can be understood from the previous discussion that h_Y is always a lower boundary of the critical field

$$h_{c1} \geq 1 + \alpha - 3A_1^2, \quad \Delta < 0. \quad (7)$$

If we increase A_1 while keeping α fixed, h_Y eventually becomes negative (as is the case for $A_1=0.8$; dash-dotted curve in Fig. 1) and we can generally not conclude using this small unit cell configuration. The reader should keep in mind that the regime where A_1 becomes large is not well described by our initial Hamiltonian (1) since in that case one should include the effects of the lattice also in the NNN interactions.

We shall now focus on the state observed in the high-field region to find the corresponding upper critical field h_{c2} above which the plateau disappears. By comparing h_{c1} to h_{c2}, we should be able to conclude on the existence of the 1/3 magnetization plateau. In the upper critical region, the situation is far more under control. The system can be seen to be well described by a three-spin coplanar "canted" configuration with two degrees of freedom (see Fig. 2). The energy of such a configuration is given by

$$E_{\text{canted}}(\theta_1,\theta_2) = (1+\alpha)[1 - 2U(\theta_1,\theta_2)] - \frac{A_1^2}{2}[1 + 2U(\theta_1,\theta_2)^2] - h(2\cos\theta_1 - \cos\theta_2), \quad (8)$$

where $U(\theta_1,\theta_2) = \sin\theta_1 \sin\theta_2 + \cos\theta_1 \cos\theta_2$.

The configuration UUD, which corresponds to $\theta_1=\theta_2=0$, is always a critical point of the function $E_{\text{canted}}(\theta_1,\theta_2)$. A closer look at the second-order derivatives with respect to θ_1 and θ_2 shows that it is a local minimum only for $0 \leq h \leq 1 + \alpha + A_1^2$. The other critical points satisfy the following set of equations:

$$Y = 2X, \quad (9)$$

$$h = [1 + \alpha + A_1^2(2X^2 + \sqrt{1-X^2}\sqrt{1-4X^2}\sigma_1\sigma_2)] \times (2\sqrt{1-X^2} - \sqrt{1-4X^2}\sigma_1\sigma_2), \quad (10)$$

where

$$\sin\theta_1 = X, \quad \cos\theta_1 = \sigma_1\sqrt{(1-X^2)}, \quad (11)$$

$$\sin\theta_2 = Y, \quad \cos\theta_2 = \sigma_2\sqrt{(1-Y^2)}. \quad (12)$$

The quantities $\sigma_1,\sigma_2=\pm1$ account for all the possible signs of both cosines. We see from Eq. (9) that there is a strong constraint on (θ_1,θ_2) verified regardless of the values of the couplings. At $h=1+\alpha+A_1^2$, Eq. (10) admits only one solution which turns out to be UUD. For a larger value of h, UUD can no longer be a critical point, which implies

$$h_{c2} = 1 + \alpha + A_1^2, \quad (13)$$

corresponding to the exit of the plateau in the high-field region. From this discussion it can be concluded that whenever our assumptions are correct, there is a plateau at $M_z=1/3$ of length $\Delta h_{1/3} = 4A_1^2$ starting at h_{c1}. This result has been checked to be consistent with the MC computations and the analytical value of h_{c2} matches the value estimated from all the curves in Fig. 1.

There is one more question we need to address: for which set of parameters (A_1,α) can we observe this plateau? Under the previous assumptions regarding the states observed in the low- and high-field regions, we can conclude it exists for any $A_1 > 0$. Yet the system cannot be described in such a manner for all values of α and A_1. Working at a fixed lattice coupling $A_1=0.3$, we were able to obtain some magnetization curves varying the frustration α. Some of those curves are plotted in Fig. 3, which clearly shows that there is only a narrow region in α where the plateau is observed. A precise answer to the previous question is rather challenging, and we shall first try to discuss this point in a more qualitative manner before adopting a more precise strategy. At $M_z=1/3$, we can of course expect to see many different configurations, depend-

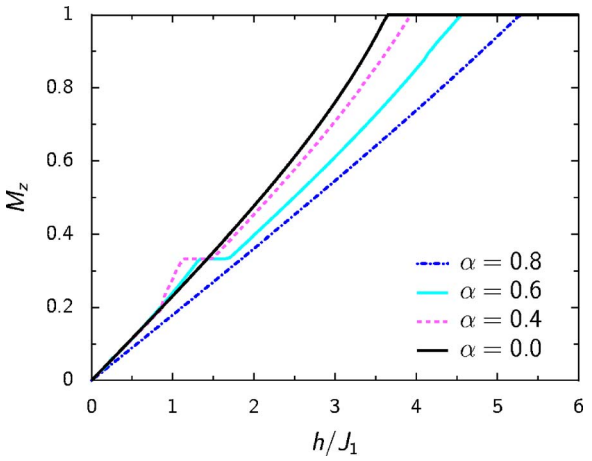

FIG. 3. (Color online) Magnetization curves $M(h)$ for $N=30$ spins with $A_1=0.3$ and $\alpha=0.0,0.4,0.6,0.8$. Periodic boundary conditions are applied on the chain. The system is gradually cooled to $T\approx 0$ over 3×10^6 Monte Carlo sweeps.

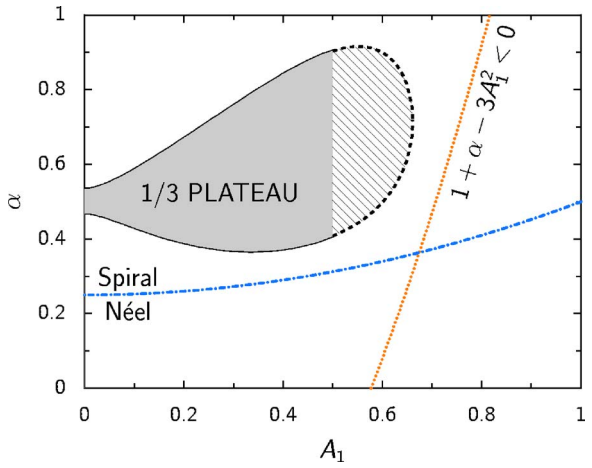

FIG. 4. (Color online) Qualitative (A_1,α) phase diagram. The filled area between the two full curves corresponds to the region of the parameters space where the $M_z=1/3$ plateau is observed. The hatched region between the two dashed curves is the region of the parameters space for which our approach is no longer observed to be fully valid. Also represented, the limit between Néel and spiral ground states at $h=0$ (dash-dotted line) and the region where $1+\alpha-3A_1^2<0$ (dotted line).

ing on the values of the couplings. However, the MC simulations suggest that the plateau always corresponds to the UUD configuration. This state is perfectly collinear, minimizing the quartic contribution to the effective Hamiltonian (2). For instance, it can be seen numerically that for $\alpha=1/2$ with no coupling to the lattice, the system reaches 1/3 magnetization in the UUD configuration. Even a small positive value of A_1 will then stabilize the UUD state enough for it to be stable when the field is slightly increased. On the opposite, if one antiferromagnetic coupling dominates the other, the system will be in a different state at $M_z=1/3$. In the extreme case where $\alpha\approx 0$ for instance, the system will favor Néel order in the xy plane, each spin having the same z-axis projection $S_z=1/3$. This layout already trades off some collinearity in favor of magnetic field alignment. There is no surprise that this trade-off will be further enhanced as the magnetic field is increased, so that no plateau should be observed.

A more accurate way to tackle this issue is to start from the $h=0$ spiral ground state and ponder over the state adopted by the system when the magnetic field increases. We have already performed part of this task earlier, suggesting that the system slowly moves to a "Y" configuration, whose out-of-plane components make it a "precursor" of the UUD configuration. Another plausible solution is that the spins, while keeping their spiral structure in the xy plane, all acquire the same S_z projection. In this case, the nth spin reads

$$\boldsymbol{S}_n = (\sqrt{1-z^2}\cos(n\theta), \sqrt{1-z^2}\sin(n\theta), z), \tag{14}$$

with $\cos\theta = 1/(A_1^2-4\alpha)$. The energy per site

$$E_{sz}(z) = z^2 + (1-z^2)\cos\theta + \alpha[z^2 + (1-z^2)\cos 2\theta] - \frac{A_1^2}{2}[z^2 + (1-z^2)\cos\theta]^2 - hz \tag{15}$$

can be minimized with respect to z to find the lowest energy configuration at a given magnetic field. Our idea is to perform this minimization at $h=h_{c1}$, and to see if the corresponding configuration is of lower energy than UUD at the same field. If so, the system will not enter the plateau at h_{c1}, and of course, as mentioned in the previous paragraph, no plateau should be observed. For a fixed value of A_1, we can determine the range in α leading to UUD at h_{c1}. The roots of the polynomial equation are evaluated numerically, from which we sketch the phase diagram represented in Fig. 4. This approach only makes sense when we have a precise value for h_{c1}, which we saw is the case if A_1 is not too large ($A_1 \lesssim 0.5$ from the MC data). We notice that the diagram is in agreement with the situation depicted in Fig. 3, as well as the one in Fig. 1, when A_1 is not too large. The most remarkable feature is that for an arbitrarily small, yet strictly positive A_1, one can find a value of α for which the plateau phase is observed.

The effect of temperature on the magnetization plateau is potentially important as an "order by disorder" effect[19] could further stabilize the plateau. We investigated this point by performing our MC simulations at different temperatures, without annealing the system. A sample is given in Fig. 5, and in general we observed no remarkable features. The increasing thermal fluctuations quickly destroy the plateau. We should also mention that we observed no strong finite-size effects in the numerical simulations, which is why we were always able to work on systems with less than a hundred spins.

We conclude this section by focusing on the lattice deformations. Until now, we studied the effective spin-only Hamiltonian (2) which embodies the straightforward analytical approach to the problem. It is, however, important to get more insight on the structure of the lattice deformation inside the plateau phase. For that matter, we modified our MC algorithm to take into account the lattice degrees of freedom as well. Starting from the Hamiltonian (1), we used the Metropolis algorithm for both the spin positions and orienta-

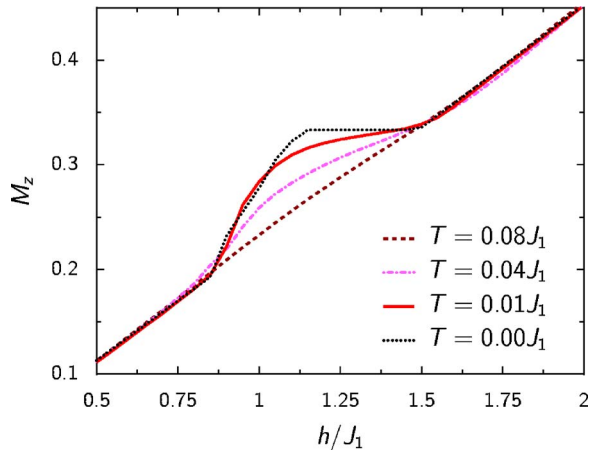

FIG. 5. (Color online) Magnetization curves $M(h)$ for $N=30$ spins with $A_1=0.3$ and $\alpha=0.4$ around $M_z=1/3$ for different temperatures $T=0,0.04,0.08$ in units of J_1. Averages are computed on 2^{22} sweeps through the lattice after an initial 2^{18} sweeps of thermalization. Increasing the temperature quickly destroys the plateau observed at $M_z=1/3$.

tions, applying periodic boundary conditions on the chain. We studied the normalized histograms of the displacements δ_i at finite temperature. We fixed $\alpha=0.4$ and $A_1=0.3$, the same values used in Fig. 5 to allow a direct comparison between the two figures, and selected the magnetic field so that the system is at $M_z\approx 1/3$. Besides the value of $A_1=\tilde{A}_1/\sqrt{K}$, we need to give K, the spring constant in Eq. (1), a sensible value. We took $K=10^3J_1$, large enough to make sure the displacements remain small. This corresponds to $\tilde{A}_1\approx 9.5$. We mention that both K and A_1 are of the same order of magnitude as the one for a more complex two-dimensional material such as $SrCu_2(BO_3)_2$ (Ref. 7) and that they can be considered at least as "realistic" for copper germanate or lithium vanadate.[21] The results are given in Fig. 6.

We see that the lattice deformations are not uniform and that their histogram presents two peaks at $T=0.01J_1$. They

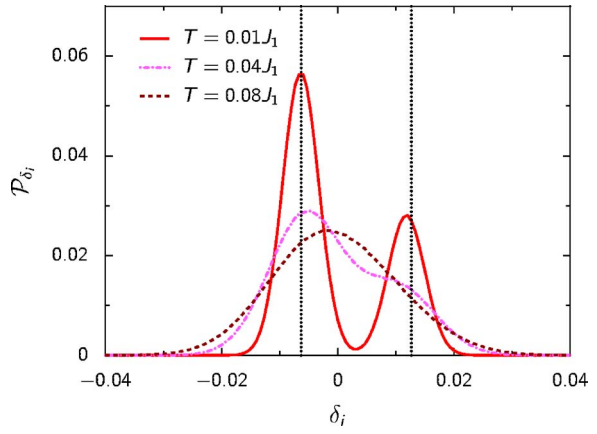

FIG. 6. (Color online) Normalized lattice displacement histograms for $N=30$ spins with $\alpha=0.5$, $A_1=0.4$ ($K=10^3J_1$), and $h=1.5$ at different temperatures. 300 points were used in the interval $[-0.1,0.1]$. The two dotted vertical lines correspond to the $T=0$ limit calculated in the text. The data were obtained using a direct classical Monte Carlo for the Hamiltonian (1).

are centered around a negative and positive value of the displacement δ_i. This suggests that the underlying deformation consists of up-down-up (UDU) trimers on the chain. Let us introduce δ_+ the displacement between two consecutive trimers and δ_- the displacement between the down spin and its two nearest neighbors inside the trimer. The energy of this unit cell is given by

$$E = 3K\delta_-^2 + 4J_1\tilde{A}_1\delta_- - J_1 + J_2 - H, \tag{16}$$

where the periodic boundary conditions imply $\delta_+=-2\delta_-$. Minimizing the energy, the deformation should become

$$\delta_+ = -2\delta_- = \frac{4\tilde{A}_1J_1}{3K} \tag{17}$$

at $T=0$ K. Going back to Fig. 6, at $T=0.01J_1$ the distribution clearly exhibits two peaks and we can see that they are almost centered around δ_+ and δ_-, respectively. The ratio between the height of the two peaks is about 2, a consequence of the fact there are twice as many up spins than down spins in the UUD state. Those results seem to validate the trimer scenario at low temperature. When the temperature increases to $T=0.04J_1$, the peaks start to overlap, betraying the gradual destruction of the plateau already seen in Fig. 6. Finally at $T=0.08J_1$, we end up with a single peaked almost-Gaussian distribution: the plateau eventually disappeared. We end up by stating that the expectation value of the displacement is always zero as the periodic boundary conditions applied ensure the length of the chain remains fixed throughout the simulation.

III. TRANSITION TO SATURATION

The study of the upper critical magnetic field yields another interesting result: we can get a precise picture of how the system eventually reaches saturation. This result can be foreseen using classical MC, which shows that the canted state describes the system quite well even for $h>h_{c2}$. A close look at Fig. 1 shows that two different behaviors of the magnetization between h_{c2} and the saturation value are observed. For different values of spin-phonon coupling, the system can undergo a first- or second-order transition to reach saturation. We are going to demonstrate that this result can be derived from energetic considerations on the canted state. From Eq. (8), we see that the saturated state, reached for $\theta_1=0$ and $\theta_2=\pi$, minimizes the energy for a magnetic field greater than $h_{c3}=3(1+\alpha-A_1^2)$. This imposes a lower boundary on the saturation field h_U. We assume that the couplings A_1 and α are such that $h_{c2}<h_{c3}$, a situation where the previous discussion on the existence of the 1/3 magnetization plateau still holds. To be consistent with the state of system for $h>h_{c2}$, we set $\sigma_1=1$ and let $\sigma_2=-\sigma$ take the values ± 1 so as to be able to move from UUD to saturation continuously. At a given magnetic field, one can obtain the corresponding critical configurations by finding the roots of Eq. (10). This task reduces to the study of the two functions h_σ;

$$h_\sigma(X) = [1+\alpha+A_1^2(2X^2-\sqrt{1-X^2}\sqrt{1-4X^2}\sigma)] \times (2\sqrt{1-X^2}+\sqrt{1-4X^2}\sigma). \tag{18}$$

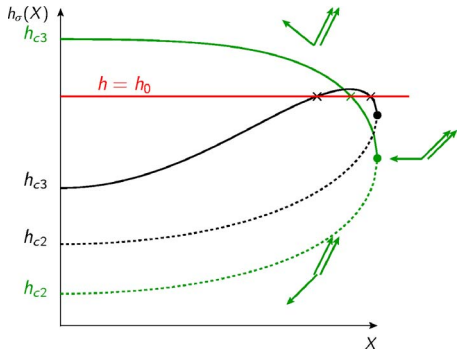

FIG. 7. (Color online) Low magnetization (dashed) and high magnetization (solid) curves as functions of $X=\sin\theta_1$ for $\alpha=0.5$, $A_1=0.5$ in green (dark gray), and $\alpha=0.5$, $A_1=0.8$ (black). The typical shape of the minima's unit cell along the green curves are depicted in the different magnetic field regions. The intersections (crosses) with the horizontal line $h=h_0$ in red (gray) gives the competing critical point at this magnetic field. The colored dots correspond to the minimal configuration with one spin in the xy plane.

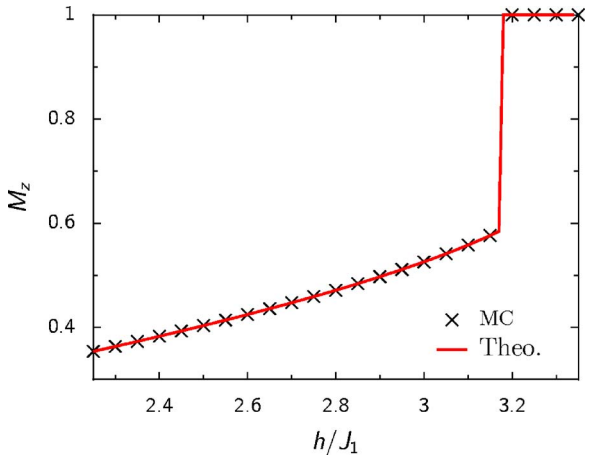

FIG. 8. (Color online) Upper region of the magnetization curve for $\alpha=0.5$ and $A_1=0.8$ at $T=0$. The full line represents the results obtained using the analytical minimization of the canted state energy. Crosses represent the data obtained by Monte Carlo.

Their roots can be determined graphically for a fixed field h_0 as they are the values of X for which the line $h=h_0$ intersects $h_\sigma(X)$. The "low magnetization" function h_- will give us solutions with one spin still pointing down, whereas the "high magnetization" function h_+ will give us states where all the spins have a positive S_z component. Figure 7 is a plot of both functions for two sets of values α, A_1. In both cases, the curves for h_+ and h_- join at $h_{c4}=\sqrt{3}(1+\alpha+A_1/2)$ (dots as shown in Fig. 7). For this value of the magnetic field, the root of h_σ corresponds to a configuration in which one of the three spins lies precisely in the xy plane. Two possible behaviors are observed. For instance, when $\alpha=A_1=0.5$ [which corresponds to the green (dark gray) curves in Fig. 7], we see that for a fixed magnetic field $h\in[h_{c2},h_{c3}]$ there is only one critical point of the energy, which can be shown to be a minimum. We are able to follow easily the state of system as the magnetic field increases. The two up-spins first slightly tilt to let the down-spin reach the xy plane and then they all progressively align along the z axis while still satisfying Eq. (9). The three-spin unit cell configuration smoothly goes from UUD to saturation.

For $A_1=0.8$ (black curves as shown in Fig. 7), the "high magnetization" function h_+ (solid black curve as shown in Fig. 7) presents a maximum. In this case, three states are potentially competing for h between h_{c3} and its maximum value: the saturated state and the two roots of h_+. We ought to compare their energies to conclude, but it is not surprising that the outcome can be a first-order transition to saturation. We numerically solved the analytical equations involved to get the magnetization curve from the exit of the plateau to saturation for $A_1=0.8$. The saturation field we obtain is $h_U \approx 3.17063$, for which the system jumps from $M_z\approx 0.58434$ to saturation. The comparison between this minimization and the MC data is given in Fig. 8 and shows the excellent agreement achieved.

A more in-depth study of the h_σ functions' extrema allows us to work out the range in (α, A_1) for which the transition to saturation is of first or second order. The former, which are related to the existence of a nontrivial maximum in h_+, occur only if $1\leq(1+\alpha)/A_1^2\leq\frac{11}{2}$ in agreement with our numerical observations.

Finally, it can be pointed out from Eq. (18) that for $X=1/\sqrt{5}$, the function h_+ no longer depends on the coupling A_1. This state (if reached) will be the minimum of the canted configuration energy for a magnetic field

$$h_\times = \frac{5}{\sqrt{5}}(1+\alpha). \tag{19}$$

At this field the magnetization is $M_z=M_\times=5/(3\sqrt{5})$. This explains why for our selection of parameters, all the curves except one in Fig. 1 cross at a field whose estimate, given in Sec. II, coincides with $h_\times$. Regardless of the value of A_1, if the system is not saturated at $h_\times$, then its magnetization will always be $M_\times$.

IV. SUMMARY AND CONCLUSION

The effect of lattice deformations at the classical level in a frustrated spin system has been illustrated working on a simple J_1-J_2 spin chain coupled to adiabatic phonons. We provide an overall picture of the magnetization properties for a large set of the parameters α, A_1 introduced in our model. We have found that a plateau at $M_z=1/3$ is present in a certain region of the parameter space, while no other plateaus are observed. Frustration is a necessary ingredient, as the plateaus can only arise when the zero-field ground state is a spiral. The other ingredient, the coupling to lattice deformations, is such that for an arbitrarily small, yet strictly positive A_1, one can find a value of α for which the plateau phase is beheld. Further increasing A_1 will broaden the region in the parameter space for which the plateau occurs, until the effective coupling is no longer mild enough for our analytical approach to be valid, even if a numerical approach is still achievable. It should be emphasized that the stabilization mechanism is purely energy driven and triggered by the quartic interaction induced by the lattice coupling in the effective Hamiltonian (2). The underlying lattice deformation

shows the chain is made of UDU trimers inside the plateau phase.

The absence of plateaus at $M_z=0$ and $M_z=1/2$ in the classical model as compared to the quantum case can be understood by analyzing the ground-state structure of the plateaus in the quantum case. It is only for $M_z=1/3$ that one observes a classical type of spin configuration, of the UUD type, while in the other cases a quantum state is apparent.

ACKNOWLEDGMENTS

We thank A. Dobry, A. Honecker, P. Holdsworth, and T. Vekua for helpful discussions. This work was partially supported by ECOS-Sud Argentina-France collaboration (Grant No. A04E03) and PICS CNRS-CONICET (Grant No. 18294).

[1] D. C. Cabra and P. Pujol, *Field Theoretical Methods in Quantum Magnetism*, Lecture Notes in Physics Vol. 645 (Springer-Verlag, Berlin, 2004).
[2] S. R. White, Phys. Rev. Lett. **69**, 2863 (1992).
[3] U. Schollwöck, Rev. Mod. Phys. **77**, 259 (2005).
[4] *Density Matrix Renormalization: A New Numerical Method*, Lecture Notes in Physics No. 528, edited by I. Peschel, K. Hallberg, X. Wang, and M. Kaulke (Springer, New York, 1999).
[5] G. Misguich and C. Lhuillier, *Two-dimensional Quantum Antiferromagnets*, edited by H. T. Diep (World Scientific, Singapore, 2005).
[6] A. Auerbach, *Interacting Electrons and Quantum Magnetism* (Springer-Verlag, New York, 1994).
[7] S. Miyahara, F. Becca, and F. Mila, Phys. Rev. B **68**, 024401 (2003).
[8] K. Penc, N. Shannon, and H. Shiba, Phys. Rev. Lett. **93**, 197203 (2004).
[9] M. F. Thorpe and M. Blume, Phys. Rev. B **5**, 1961 (1972).
[10] M. Blume, P. Heller, and N. A. Lurie, Phys. Rev. B **11**, 4483 (1975).
[11] J. Stephenson, J. Math. Phys. **17**, 1645 (1976).
[12] T. Vekua, D. C. Cabra, A. Dobry, C. Gazza, and D. Poilblanc, Phys. Rev. Lett. **96**, 117205 (2006).
[13] K. Hida, J. Phys. Soc. Jpn. **63**, 2359 (1994); K. Okamoto, Solid State Commun. **98**, 245 (1996).
[14] J. P. Boucher and L. P. Regnault, J. Phys. I **6**, 1939 (1996).
[15] M. Isobe and Y. Ueda, J. Phys. Soc. Jpn. **65**, 3142 (1996).
[16] N. Fujiwara, H. Yasuoka, M. Isobe, Y. Ueda, and S. Maegawa, Phys. Rev. B **55**, R11945 (1997).
[17] J. Riera and A. Dobry, Phys. Rev. B **51**, 16098 (1995).
[18] C. Kittel, Phys. Rev. **120**, 335 (1960).
[19] J. Villain, R. Bidaux, J. P. Carton, and R. J. Conte, J. Phys. (Paris) **41**, 1263 (1980).
[20] I. Affleck and K. Hida, J. Phys. Soc. Jpn. **74**, 1849 (2005).
[21] F. Becca, F. Mila, and D. Poilblanc, Phys. Rev. Lett. **91**, 067202 (2003).